Title

Shape Memory Polyurethane-Based Smart Polymer Substrates for Physiologically Responsive, Dynamic Pressure (Re)Distribution

Journal

ACS Omega, 4(13)

ISSN

2470-1343

Authors

Kumar, Bipin
Noor, Nuruzzaman
Thakur, Suman
et al.

Publication Date

2019-09-24

DOI

10.1021/acsomega.9b01167

Peer reviewed

ACS OMEGA

Article

Cite This: ACS Omega 2019, 4, 15348−15358

http://pubs.acs.org/journal/acsodf

Shape Memory Polyurethane-Based Smart Polymer Substrates for Physiologically Responsive, Dynamic Pressure (Re)Distribution

Bipin Kumar,[†] Nuruzzaman Noor,*[,‡] Suman Thakur,[‡] Ning Pan,[⊥] Harishkumar Narayana,[‡] Siu-cheong Yan,[§] Faming Wang,[‡] and Parth Shah[∥]

[†]Department of Textile Technology, Indian Institute of Technology Delhi, Hauz Khas, New Delhi 110016, India

[‡]Institute of Textiles and Clothing, [§]University Research Facility in Chemical and Environmental Analysis, and [∥]School of Design, The Hong Kong Polytechnic University, Hung Hom, Kowloon, Hong Kong SAR, China

[⊥]Biological & Agricultural Engineering, UC Davis, Davis, California 95616, United States

Supporting Information

ABSTRACT: Shape memory polymers (SMPs) are an exciting class of stimuli-responsive smart materials that demonstrate reactive and reversible changes in mechanical property, usually by switching between different states due to external stimuli. We report on the development of a polyurethane-based SMP foam for effective pressure redistribution that demonstrates controllable changes in dynamic pressure redistribution capability at a low transition temperature (~24 °C)—ideally suited to matching modulations in body contact pressure for dynamic pressure relief (e.g., for alleviation or pressure ulcer effects). The resultant SMP material has been extensively characterized by a series of tests including stress−strain testing, compression testing, dynamic mechanical analysis, optical microscopy, UV−visible absorbance spectroscopy, variable-temperature areal pressure distribution, Fourier transform infrared spectroscopy, Raman spectroscopy, X-ray diffraction, differential scanning calorimetry, dynamic thermogravimetric analysis, and ^{1}H nuclear magnetic resonance spectroscopy. The foam system exhibits high responsivity when tested for plantar pressure modulation with significant potential in pressure ulcers treatment. Efficient pressure redistribution (~80% reduction in interface pressure), high stress response (~30% applied stress is stored in fixity and released on recovery), and excellent deformation recovery (~100%) are demonstrated in addition to significant cycling ability without performance loss. By providing highly effective pressure redistribution and modulation when in contact with the body's surface, this SMP foam offers novel mechanisms for alleviating the risk of pressure ulcers.

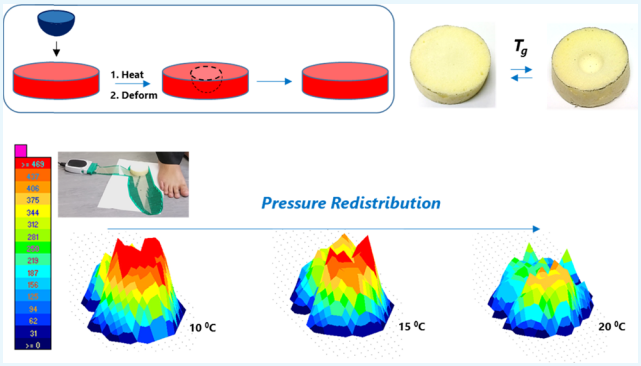

1. INTRODUCTION

Shape memory polymers (SMPs) can temporarily and securely hold a deformed shape but recover to an original, "true" shape, in response to an external stimulus such as temperature, pH, etc.[1−8] This unique "shape memory effect" comprises shape fixity and shape recovery (Figure 1). Shape fixity enables acquisition of a temporary, deformed shape via a suitable programming process, whereas shape recovery retrieves the original shape via controlled application of a stimulus.[9−12] This shape controllability (i.e., fixity or recovery) is currently at the forefront of multiple research domains spanning biomedical,[13−17] textiles,[18−20] aerospace,[21,22] etc. Primarily in biomedical, SMP are attractive in critical applications including sutures,[23] stents,[24] embolic biomedical devices,[25] drug delivery devices,[26,27] tissue scaffolds,[28,29] and compression stockings.[30−33] To further extend understanding of such materials, this study will systematically characterize the use of porous, open-cell SMP foams as smart contact surfaces for controlled, dynamic pressure (re)distribution on the human body.

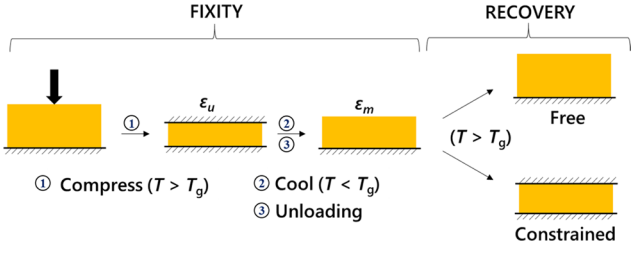

Figure 1. Diagram of the volume changes expected in shape fixity and recovery processes of shape memory polymers, below or above the polymer glass-transition temperature, T_g, upon application and/or removal of an external pressure constraint.

Pressure ulcers/injuries arise when uncontrolled, uneven, and prolonged pressure distribution between the body and

Received: April 23, 2019
Accepted: September 2, 2019
Published: September 12, 2019

DOI: 10.1021/acsomega.9b01167
ACS Omega 2019, 4, 15348−15358

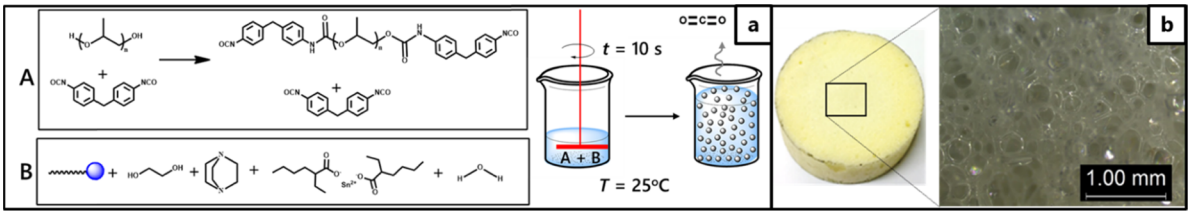

Figure 2. (a) Schematic of the shape memory polymer foam preparation process involving step A: Formation of a "prepolymer" through mixing of 4,4′-methylene diphenyl diisocyanate (MDI) and poly(propylene glycol), followed by step B: Mixing of the prepolymer with ethylene glycol (EG), amine and tin catalysts as well as H_2O, prior to carrying out the foaming and curing processes. (b) Pore structure and size distributions of the microcellular shape memory polyurethane polymer foam as observed by optical microscopy.

support surface generates localized regions of high pressure.[34] High pressure damages soft tissue, especially near bony prominences due to their low curvature, and significantly compresses vascular networks, decreasing the supply of oxygen and essential nutrients, resulting in tissue ischemia and, finally, tissue breakdown. The resultant chronic ulcers may cause significant pain, discomfort, decreased quality of life, and, when associated with superimposed infection, may even lead to death.[35,36] Despite several available, yet oft-ineffective ulcer treatment measures, the first, most basic preventive and recommended action is to reduce the interfacial pressure between the skin and support surface.

Pressure distribution is the dispersion of localized peak pressure or shear forces over larger areas. Usually, it is carried out by either; (i) a reactive surface (e.g., foam or gel mattresses) where pressure reduction occurs through increased contact area, or (ii) an active surface that repositions body weight by periodically shifting the contact area via alternate inflation and deflation of a series of air-filled bladders. Both have questionable efficacy, and many challenges still exist in current medical practice:

(A) Contemporary foam-based reactive surfaces primarily exhibit passive pressure reduction; they have fixed immersion (extent of allowing the body to sink into the surface) and envelopment (ability to conform to bodily contours, especially around anatomical landmarks, e.g., heel, sacrum, coccyx, etc.).[37−41] Thus, it is virtually impossible for such modalities to achieve adjustable pressure distribution, if required.

(B) Currently available dynamic air mattresses fail miserably in envelopment. They are also costly, complicated in design, and noisy in use.

(C) No currently available surface can combine both active and reactive functions, for selective response to patient needs.

(D) Although manual repositioning of patients aids pressure relief, it is tedious and labor-intensive, placing unduly heavy burdens on medical care providers.

SMP foams are the focus of this paper due to their low density, high compressibility, flexibility, softness, and wearer comfort, potentially ideal as a cushioning, contouring, responsive, and material that can be easily processed. Open-celled structures potentially offer greater comfort due to their higher air and moisture permeabilities compared to closed-cell structures (e.g., syntactic foams).[42−46] The unique stimulus-responsive and dynamic shape-change properties of SMP could solve some of the pressure redistribution challenges.[47−50] The nature of the foam material (i.e., the firmness or softness) tends to determine the pressure generated on the body's surface.[51,52] Current commercial cushioning materials (e.g., sleeping mattresses, shoe insoles, car seats, etc.) have a fixed stiffness, meaning they are completely unsuited for externally responsive pressure modulation. Conversely, SMP demonstrates a notable modulus change in response to a variable external stimulus, typically heat.[53,54] Such changes are superior to conventional polymers in their mechanical and thermodynamical properties around the (glass) transition temperature (T_g here, ∼24 °C) tuned around the SMP normal working temperature (here, ∼20 °C). Thus, above T_g, the SMP behaves rubbery, elastic, and soft; below T_g, it becomes hard and displays glassy behavior. Such reversible firmness change properties are ideal for matching to body temperature fluctuations.[54] Additionally, SMP shape fixity properties can be further exploited to reshape the selecting part of a foam substrate for maximal immersion and envelopment.

This paper will explore the use of SMP foams as reactive and smart surfaces for pressure distribution, using insoles and foot pressure redistribution as an illustrative application. Plantar pressure redistribution is important because localized and prolonged plantar pressure leads to chronic pressure sores, nonhealing wounds, and ultimately results in foot ulceration, with further potential limb loss in high-risk groups, e.g., diabetic patients, sufferers of muscular dystrophy, and the elderly.[55−58] Lightweight and flexible orthotic foams can reduce fatigue, relieve pressure, and increase circulation by evenly redistributing normal and shear stresses arising from bodily weight along the length and breadth of the foot, for personalized comfort and support.[59] Broadly, two possible methods exist for utilizing SMP foam shape fixation for pressure redistribution: (i) Shaped fixing, where a predetermined shape is achieved prior to foot application; the coverage area is increased to reduce pressure. There is no temperature fluctuation for pressure relief and foam T_g > 50 °C so there is little shape change if the foot temperature increases; (ii) Redistribution of pressure points, where the fixed shape is used but temperature fluctuation is done externally in the foot to selectively release the contact stress or pressure. This shifts pressure points naturally, preventing excessive stress during plantar loading, especially over sensitive areas (e.g., bony prominences),[59] and the actuation range of the foam will be lower (∼30−50 °C). This paper will systematically characterize thermally actuated SMP foams as used for dynamic plantar pressure redistributive applications.

2. RESULTS AND DISCUSSION

2.1. Shape Memory Polyurethane (SMPu) Polymer Foam Synthesis. Shape memory polyurethane (SMPu) foam was synthesized using the gas foaming technique where a chemical blowing agent (i.e., water) reacts with isocyanate monomers to produce carbon dioxide (Figure 2a).[60,61] The

DOI: 10.1021/acsomega.9b01167
ACS Omega 2019, 4, 15348−15358

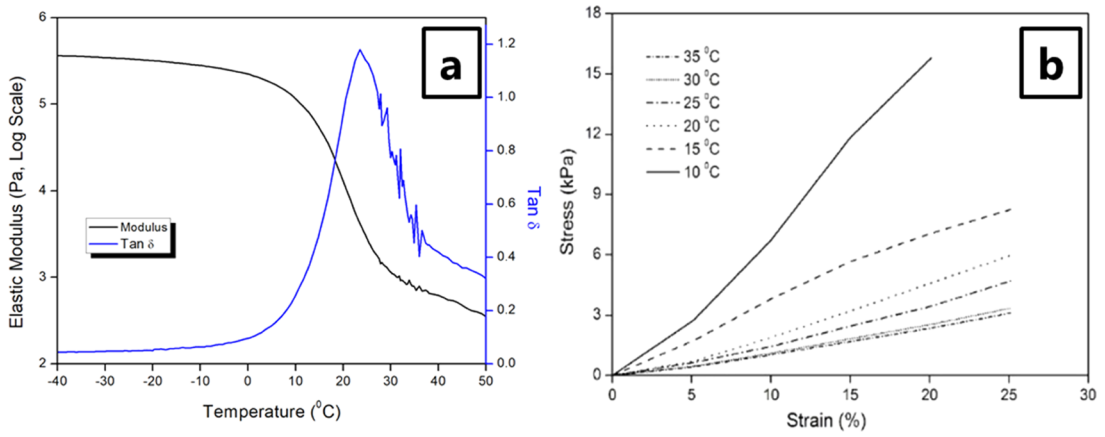

Figure 3. (a) Results of dynamic mechanical analysis (DMA) testing on SMPu foams indicating the elastic modulus and tan δ responses respectively in response to a controlled variation in temperature. (b) Compressive stress−strain results for SMPu foams at different temperatures.

novelty of this synthetic work is that this poly(propylene glycol) (PPG)−poly(ethylene glycol) system for different methods for pressure control has not been explored previously. After foaming, the open-cell SMPu samples were cured for a further 24 h in air at 80 °C. Such samples were subsequently characterized and tested without further treatment, against a thermoplastic polyurethane (TPU) reference material. Figure 2b shows the SMPu foam structure where released CO_2 gas promoted self-assembly of a porous architecture with good interconnectivity.[9] The SMPu foam density was 64.7 kg m^{-3}, with a porosity of 94% and pore size range of 0.1−0.5 mm.

2.2. Shape Memory Polyurethane Polymer Foam Bonding Interactions and Materials Characterization. All expected thermoplastic polyurethane signals were observed in the attenuated total reflectance (ATR)-Fourier transform infrared (FTIR) spectra. Additional assignments (see Figure S3, Supporting Information (SI)) indicate clear differences between the TPU and SMPu foam concerning incidence and intensity of IR bands, due to the partial degradation of TPU as well as the organic reactants used to form the SMPu foam.[62−64] The shift of certain bands (N−H, C═O, and C−O stretches of TPU are shifted to lower wavenumbers for SMPu foam) indicates increased hydrogen bonding effects in the hard segments.[65,66] Such differences are caused by the changes made to the parent TPU structure upon mixing with MDI and other components, during the SMPu foam formation process. These structural changes cause modifications of, e.g., modulus, stiffness, etc., and thus facilitate the reversible shape memory properties. For example, there are a greater number of signals for −CH stretches and bends as well as shifted and changed band profiles at 1729 cm^{-1}, representing hydrogen-bonded carbonyl stretching components (−C═O) of the urethane ester groups and corroborated by the C−O−C moiety at 869 cm^{-1}, for the SMPu foams. Likewise, a smaller shoulder at 3450 cm^{-1}, present in the bands for the SMPu foams but absent in the parent TPU, is consistent with non-hydrogen-bonded urea and urethane N−H groups, possibly from the amine catalysts.

There is broad Raman band position agreement between TPU and SMPu foam (see Figure S4, SI). Data were acquired both above and below the T_g; data below the T_g for the SMPu foam were acquired while the sample has a constrained, temporarily fixed shape, to ensure the sub-T_g condition. While structural disorder revealed by a shift in temperature around the T_g is expected, only moderate changes in detected bonding interactions were observed here.[63,67−70] The SMPu foam shows increased relative intensity for the H-bonded urethane stretch (1706 cm^{-1}), believed to be due to the disordered hard segments of poly(urethane urea) dispersed in the soft-segment phase.[71] In addition to increased band intensities, there are several shifted or absent bands for the SMPu foams versus the TPU reference. Both 977 and 865 cm^{-1} (both C−O−C) bands are absent, while the 1439 cm^{-1} (C−H) and 1048 cm^{-1} (C−O) bands are shifted, for the foam. This indicates the additional formation of chemical interactions thought to be induced by the presence of oxygen functional groups and/or additional disorder-related defects. Finally, the SMPu foam shows further weak band(s) at <300 cm^{-1}; in the 235−295 cm^{-1} region, which is completely absent for the TPU and likely corresponds to aliphatic chains, possibly arising from the use of linkers or blowing agents in the formation of the SMPu foams. Proton nuclear magnetic resonance (^{1}H NMR) confirms that the broader SMPu foam chemical structure is heavily dependent on the precursor mixture components and ratios used (see Figure S5 and refer to Table 1). Signals at 7.074 and 7.248 ppm conform to the H_a and H_b of the MDI precursor aromatic ring; the presence of PPG precursor indicated by shifts at 4.992 ppm (CH group) and 1.571−1.119 ppm (signals of CH_3 protons at slightly different chemical environment); and the signals at 3.5−3.2 ppm from the CH_2 protons of the EG precursor.[72,73]

The differential scanning calorimetry (DSC) curves (second heating) of the SMPu foam, (see Figure S6, SI), probing the crystallinity show no significant inflection point, peak, or step change in the DSC curves of either the as-synthesized SMPu foam or TPU (reference standard), over −80 to 100 °C that would otherwise indicate a kinetic change at the T_g.[74,75] This is a known problem for medical-grade urethanes and other highly cross-linked materials, where the T_g often becomes flat and diffuse such that it cannot be seen in DSC.[76] Dynamic mechanical analysis (DMA) data are more sensitive than DSC (up to 100 times) to changes occurring at the T_g (see Figure 3), and this corresponds to what is observed here.[76,77] This signifies that both the SMPu foam and TPU are extensively amorphous and display typically glassy behavior over the temperature range, perhaps explained by the high miscibility of hard and soft phases, smaller more imperfectly packed hard domains, and ready chain mobility.[75,78−82] This amorphous character is further affirmed by the X-ray diffraction (XRD) data (see Figure S7, SI); the diffraction patterns comprise only

DOI: 10.1021/acsomega.9b01167
ACS Omega 2019, 4, 15348−15358

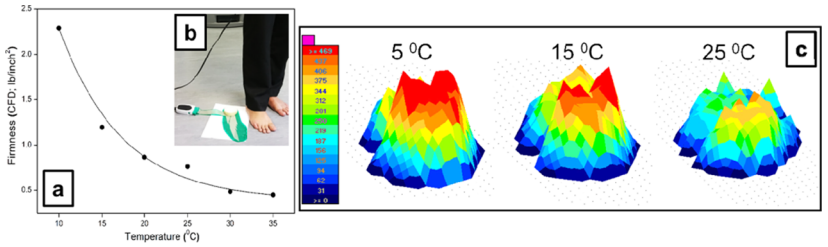

Figure 4. (a) Firmness response of the SMPu foam against temperature. (b) Tekscan *F*-scan pressure system for dynamic, variable temperature, areal pressure distribution measurement on SMPu foams in response to a static external downward force from the heel of an adult male. (c) Areal pressure distribution of the SMPu foams under different surface temperatures, upon exposure to a constant, static external downward force. (Photograph courtesy of Bipin Kumar. Copyright 2019.)

a broad amorphous peak at 2θ = 20−22° over the entire acquisition range. This amorphous behavior is as expected for segmented T_g-type TPU-based materials.[83]

Dynamic thermogravimetric analysis (TGA) curves illustrate the thermal stabilities of TPU and SMPu foams under both inert (i.e., N_2) and oxidizing (i.e., air) conditions while their first derivatives highlight degradation weight loss maxima over the 35−600 °C range (see Figure S8 and Table S1, SI). Broadly, SMPu foams exhibit simple thermal decomposition with the formation of gaseous byproducts, whereas TPU undergoes multistep decomposition. Initial weight losses (≤2%) are due to loss of adsorbed moisture and the thermolysis processes disrupting the weakest structural bonds, a well-known trait of TPU-based samples. The slightly higher SMPu foam weight loss is likely due to the greater adsorbed moisture on the foam's larger surface area as well as evaporation of components such as CO_2 and long-chain alkyl fragments from the foaming agents. The SMPu foam presents primarily a single degradation stage, whereas the pure TPU demonstrates a two-/three-stage decomposition process, in line with previous reports.[84−86] For TPU, the first decomposition stage relates to scission of the principal urethane linkages, corresponding to degradation of TPU hard segments; the second decomposition stage likely relates to degradation of the soft phase.[87−89] SMPu foams have a slightly earlier decomposition temperature onset in weight loss; the foams are less structurally thermostable due to decomposition of the present TPU parent material during foam formation as well as the decreased distinction between hard and soft segments.[90] In air, a final degradation step is found for both the SMPu foam and TPU at ca. 540−575 °C, believed to correspond to C−C and C−O bonds on the main polyurethane chain and the char formed in the previous stages. No further hydrolysis steps were observed here at elevated temperatures.[91] The final char residual weight was higher for TPU, due to part degradation of the SMPu foam during production of the initial foam.

2.3. Shape Memory Polyurethane Polymer Foam Polymer Properties Testing. The temperature-dependent mechanical properties of the SMPu polymer foam, including modulus and tan δ (efficiency of energy loss due to molecular disentanglement and rearrangements), are reported in Figure 3a. A sharp decline in elastic modulus occurs over −5 to 25 °C, in conjunction with a prominent peak in the tan δ spectrum, where the maximum indicates the glass-transition temperature; $T_{max} \equiv T_g \sim 24$ °C. The tan $\delta - T_g$ for SMPu composites is higher than that of its TPU counterpart (<0 °C); hence, unmodified TPU would be unsuitable for any kind of bodily responsive pressure redistributive scenario in reality, which is attributed to the increased free volume between polymeric chains and their greater mobility, in the foam structure.[92−95] Above the T_g, the material exhibits properties reflective of the rubbery state, indicating the transition of soft segments in the SMP network. tan δ is linked to a material's energy dissipating quality;[96] the low values in the rubbery state and high strain recovery rates observed for SMPu indicate close to ideal spring behavior.[97] These results were similar to thermomechanical compression tests conducted on the Instron tensile/compression tester, where a high compressive modulus is observed at low temperature (<10 °C), corresponding to a low force requirement, while a low modulus is found at a higher temperature (>20 °C)—0.01078 MPa (i.e., ≈10 kPa) (Figure 3b), which is still significant but orders of magnitude (10^2−10^3) lower than reported values for TPU standards (depending on elastomer composition) at room temperature in dry environments.[93,98,99]

For cushioning and pressure distribution applications, foam density and compression firmness (i.e., resistance to deformation) are the most important parameters. Foam firmness directly influences internal pressure development, and even slight changes in firmness can cause varying interactions with contacting tissue and so generate different interfacial pressures. Furthermore, foam firmness or softness is important in product design, especially for optimum pressure performance for postural control and wearer satisfaction. For example, although soft cushions (low firmness) decrease excessive compressive forces on joints, reducing ulcer risk, the excessive softness also reduces mechanical support, causing poor postural stability. Conversely, a firmer foam, with high rigidity, generates sufficient reactive forces to maintain postural stability, especially for older adults. Conventional foams, including ordinary polyurethane, do not exhibit heat-stimulated firmness modulation across a normal working temperature range, making them completely unsuited to any intended dynamic response application. Commercial products can only be altered at the production stage by modifying the chemical formulations and processing technologies. Conversely, the SMPu foam presented here as proof of concept can respond quickly and reversibly to allow a significant change in firmness over a narrow temperature range (i.e., in response to ambient heat stimuli).[100,101] The transition range of SMP can be readily tuned further to work across different temperature domains. In terms of relevance to orthotics, the SMPu reported here will be in the viscoelastic rubbery state for the projected duration and conditions of operation, exhibiting a springy, puttylike behavior that is ideal for pressure relief and support. The extended presence of the rubbery state thought to be aided by the use and presence of cross-linkers in the

DOI: 10.1021/acsomega.9b01167
ACS Omega 2019, 4, 15348−15358

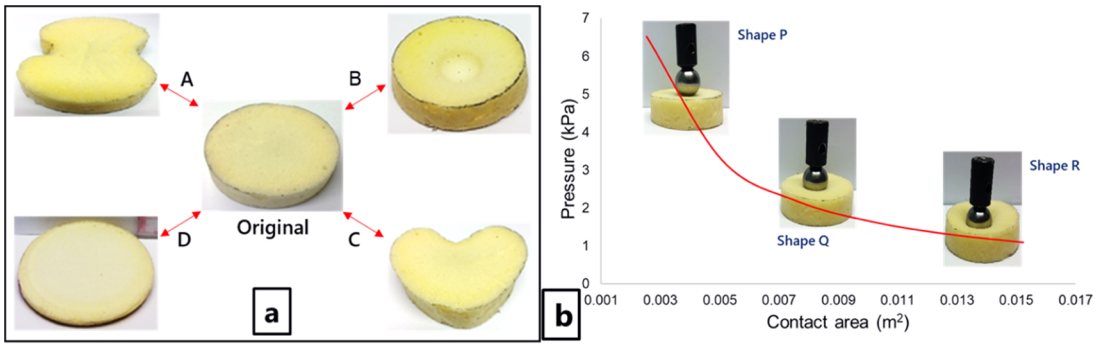

Figure 5. (a) Various programmed temporary shapes (A−D) from an SMPu foam (original) upon application of an external constraint at $T > T_g$ and then cooling the constrained shape down to $T < T_g$ to "fix" the desired temporary shape. (b) Pressure distribution of the programmed shapes (P−R) with varying surface troughs indicating variations in interfacial contact area with the spherical indenter. (Photograph courtesy of Bipin Kumar. Copyright 2019.)

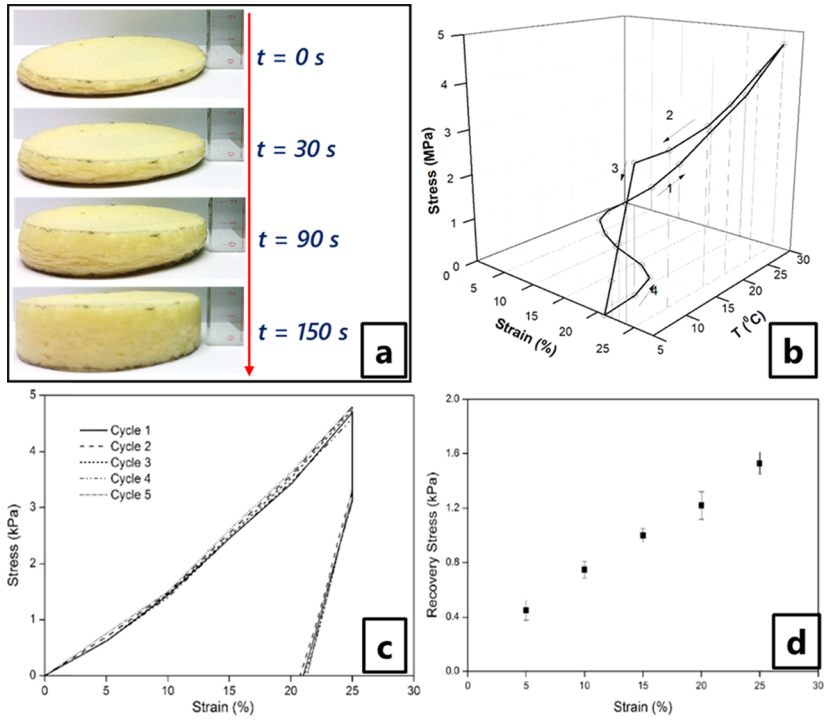

Figure 6. (a) Timed shape recovery process from a compressed SMPu foam (∼25% overall volume) to completely uncompressed (i.e., 100% volume) upon application of a heat stimulus ($T > T_g$; 24 °C). (b) Three-dimensional shape memory cycle plot of stress, strain, and temperature. (c) Stress response of SMPu polymer foam in the thermomechanical cycles of fixing and recovery upon application known strain rates. (d) Recovery stress of SMPu polymer foam for different programmed strain rates. Programming and recovery conditions; step 0: heating of specimen above T_g (30 °C); step 1: application of compressive load at high temperature to a strain value (5−50%); step 2: cooling the specimen to 50 °C; step 3: release of constraint to fix the deformed shape, and; step 4: heat the specimen to 30 °C without any constraint. (Photograph courtesy of Bipin Kumar. Copyright 2019.)

polymer system, extends the rubbery plateau and delays transition to viscous and fluid states.[102]

Figure 4a shows the influence of temperature on SMPu foam firmness, expressed in compression force deflection (CFD; the pressure (lb in.$^{-2}$) needed to compress to 25% of the specimen height). A sharp increase (up to 200%) in CFD is noted when the temperature is varied within the SMPu transition range,[30] lowering from 25 to 10 °C. Lower CFD values indicate a softer foam of smaller compression modulus, while higher CFD numbers stage firmer response with high modulus. A soft SMPu foam deforms easily, providing more interfacial contact area (i.e., higher immersion) to cover body contours for pressure reduction (i.e., higher envelopment).

This firmness variability was further validated using a Tekscan F-scan foot pressure measuring system to examine the pressure distribution of the SMPu foam by altering the temperature (Figure 4b,c). At lower temperature (≤5 °C), the SMPu foam is rigid with a high elastic modulus, due to which more pressure peaks (in red) are obtained over a concentrated region. At higher temperature (≥25 °C), the SMPu foam softens with a low modulus; a near-6-fold difference in firmness over the 5−25 °C range. Thus, the pressure is effectively redistributed and lower-pressure peaks become apparent. As such, this temperature range of operation is ideally suited for when the SMPu foam is in direct contact with anatomical

DOI: 10.1021/acsomega.9b01167
ACS Omega 2019, 4, 15348−15358

Table 1. Specific Weight Compositions of Components Required for the Formation of a Dynamically Responsive Shape Memory Polymer Polyurethane (SMPu) Foam

raw materials	chemicals specification	wt %
polyol	poly(propylene glycol) (PPG; M_n: 725; Sigma-Aldrich Chemical Company)	57.04
diisocyanate	4,4′-methylene diphenyl diisocyanate (MDI; Sigma-Aldrich Chemical Company)	38.74
cross-linker and chain extender	ethylene glycol (EG; Sigma-Aldrich Chemical Company)	2.50
blowing agent and chain extender	deionized H_2O	0.64
amine catalyst	A-1 (Shijiazhuang Chuanghong Technology Co. Ltd.) comprises 70% bis(2-dimethylaminoethyl)ether, i.e., BDMAEE: 30% dipropylene glycol	0.09
amine catalyst	A-33 (Shijiazhuang Chuanghong Technology Co. Ltd.) comprises 99% triethylenediamine	0.12
tin catalyst	Dabco T-9 (Air Product) comprises 97% stannous octoate: 3% 2-ethylhexanoic acid	0.07
surfactant	Dabco DC5179 (Air Product)	0.81

extremities, which are able to experience temperature fluctuations spanning this range.

Apart from a reversible firmness change, the SMPu foam also allows unique shape fixing and recovery properties. Through simple programming steps, the required shape can be temporarily fixed by deforming the sample at high temperature ($T > T_g$) to the target and then cooling it down to low temperature ($T < T_g$) under specific external constraints. Different shapes/concavities (A−D) were reversibly fixed from the original foam specimen under such temperature variation conditions (Figure 5a).

The pressure interaction depends on both immersion (ability to sink into the surface) and envelopment (ability to conform to the body contour) of the surface in contact. Some anatomical landmarks (e.g., heel, sacrum, coccyx, etc.) have a complex contour and are always at high risk of pressure peaks due to either poor immersion or envelopment at the contact surfaces. However, with the unique shape fixing ability of the SMPu foam, the anatomical shapes and selective contours can be readily generated directly at the site of interaction to provide greater contact area for pressure reduction and support. This pressure reduction ability was further validated to check the pressure interaction of different programmed shapes (P−R; Figure 5b). For the foam specimens fixed to different levels of spherical concavities, a higher trough from the surface (shape R) results in a larger contact with the spherical indenter and produces lower pressure compared to a shallower trough (shape P). Thus, there is an almost 80% reduction in interfacial pressure going from shape P to R.

Figure 6a shows the recovery of the original SMPu foam from a compressed state upon exposure to a heat stimulus. Once recovered, the foam can be reprogrammed to a new shape, without any residual memory effects. The whole cycle of shape fixing and recovery can be repeated multiple times, without adverse effects (Figure 6b,c).[103] The shape fixity (the ratio of the remained deformation and the maximum deformation applied) is ∼88%, and full recovery (i.e., 100% from the fixed shape to its original shape) can be observed without any loss in performance. When measured under a given constraint, i.e., a given sustained strain, the amount of recovery stress generated in the sample is indicated in Figure 6d. Almost 30% of the applied stress is stored during shape fixing, which is then released in the recovery process.

3. CONCLUSIONS

Highly responsive, shape memory polyurethane (SMPu) foams have been synthesized using a simple gas foaming technique. Biomechanical testing of the resilient, moderately deformable SMPu foams exhibits efficient pressure redistribution (∼80% reduction of interfacial pressure), stress response (∼30% applied stress stored in fixity), shape recovery properties (∼100% recovery), extended rubbery plateau, and high cycling stability to compression, of this well-investigated system, among the most impressive reported to date.[104]

While we have demonstrated highly responsive temperature actuation across the SMPu foam material on a macro scale, localized selectivity of temperature actuation across a surface must still be achieved for enhanced patient responsivity and improved outcomes. Furthermore, refinements and improved control over the gas foaming synthetic method are also needed to achieve and ensure a higher transition temperature, through variation of reaction mixture ratios and components. In addition, PU-based structures, including foams, are known to be flammable—to differing degrees depending on PU source and mixture composition (i.e., polymer chain composition, polymer density, etc). These properties can be mitigated through inclusion of flame retardants active in the condensed phase, e.g., halogenated flame retardants, inorganic fillers, carbon compounds, etc., to confer heat resistance, suppress smoke, and minimize flashover effects.[105−108] Such improvements will be the focus of future research studies.

Using the illustrative example of plantar pressure redistribution, the SMPu foam showed effective capabilities in dissipating localized pressure buildup arising from weight-bearing stress forces acting on the feet, knees, hips, and back, with progressive deformation occurring in response to increasing load, especially over/beneath bony prominences, to adjacent tissue so as to provide support and relief from discomfort, ulcers, hot spots, etc.[109] Thus, this nontoxic, low-temperature-responsive SMPu foam can facilitate preprogrammed modulation of the interface firmness and pressure to support related ergonomics, promote medical intervention, and aid wearer comfort. These findings, based on extensive characterization of the SMPu foam will be of direct relevance to diabetics, the elderly, treating bedsore ailments, sufferers of muscular dystrophy, and many other at-risk groups, while the broader principles will appeal to any involved in the smart materials and functional polymers field.

4. MATERIALS AND METHODS

4.1. Chemicals and Shape Memory Polyurethane Polymer Foam Synthesis. Details of the synthesis process for shape memory polyurethane (SMPu) foam are given in Table 1, which lists the chemical components used in foam production. The SMPu foam was produced via a prepolymer process from 4,4′-methylene diphenyl diisocyanate (MDI;

DOI: 10.1021/acsomega.9b01167
ACS Omega 2019, 4, 15348−15358

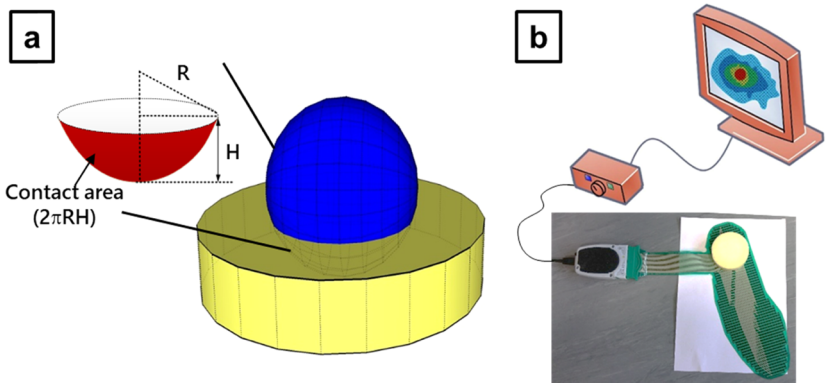

Figure 7. (a) Schematic of the response of the shape memory polymer foam upon application of an object mass of known shape and weight reflecting the contact area, used in the pressure test. (b) Image of Tekscan *F*-scan pressure measurement system setup used for pressure distribution measurement.

Sigma-Aldrich Chemical Company), poly(propylene glycol) (PPG, M_n: 725; Sigma-Aldrich Chemical Company), and ethylene glycol (EG; Sigma-Aldrich Chemical Company). The MDI and PPG were reacted in a specific molar ratio for 2 h at 80 °C to give the prepolymer. Then, the chain extender (EG) was added together with the suitable amount of amine catalyst (A-1 and A-33; Shijiazhuang Chuanghong Technology Co. Ltd., China), tin catalyst (T-9; Air Product), and surfactant (Dabco DC5179; Air Product). Diols (e.g., 1,4-butane diol or ethylene glycol) or diamines have frequently been used as cross-linkers in making shape memory polyurethane for decades.[110,111] Hydroxyl functional cross-linkers such as EG usually also serve as chain extenders, although in cases where water is present simultaneously, there are competitive effects; regardless, the hydroxyl groups of both routes will favor urethane linkage formation.[88,112,113] Deionized water (resistivity, 18 MΩ cm) was used as the chemical blowing agent for gas foaming. Mixing time was 10 s, and observed cream time was 40 s. After foaming, the sample was cured for 24 h at 80 °C.

4.1.1. Shape Memory Polyurethane Polymer Foam Material Characterization. For thermomechanical characterization, the compression tests were conducted on an Instron tester attached to a heating chamber. The compression stress, strain, and modulus were examined at a different temperature range (5−50 °C). The foam firmness was also obtained in compression force deflection (CFD), defined as the pressure (lb in.$^{-2}$) needed to compress a foam specimen by a specified percentage of its original thickness. Herein, the CFD at 25% compression was recorded at different temperatures.

Foam density was determined using standard protocols (ASTM D 1622) by cutting foam with specific dimensions and measuring its weight. Pore dimensions and distribution were examined by Leica optical microscopy (model: M165C; ASTM D 3576). The polymer thermal transition, cycling, and degradation were mapped using thermogravimetric analysis (TGA) in triplicate and differential scanning calorimetry (DSC) cycling tests. TGA measurements were carried out on a Mettler-Toledo Star e TGA Thermogravimetric Analyzer, under both air (50 mL min^{-1}) and N_2 (50 mL min^{-1}) conditions in dynamic mode, at a 10 °C min^{-1} ramp rate, over the 35−600 °C range. DSC was done on a PerkinElmer DSC 8000 under N_2 (50 mL min^{-1}) flow, over the −80 to 100 °C range, at a ramp rate of 10 °C min^{-1} and kept under hold conditions for 1 min at −50 °C. This scanning process was repeated up to three cycles, and the result of the second scan was used to obtain a transition endothermic peak. The first scan was performed to remove the residual solvent unconverted monomer. The dynamic mechanical analysis (DMA) was conducted on a PerkinElmer DMA tester to ascertain the variation in the modulus (glassy/rubbery) with temperature. Furthermore, wide-angle X-ray diffraction (WAXD) was also employed to check the crystallinity in the synthesized SMPu foam along with an ordinary thermoplastic polyurethane (TPU) as a reference. The WAXD profile was collected using a Rigaku SmartLab X-ray diffractometer with Cu Kα radiation (λ = 1.542 Å), operating at 60 kV and 60 mA, over the 2θ range of 10−40°.

Raman spectroscopy was carried out on a BaySpec Nomadic Raman Microscope, using a 785 nm laser excitation source, over the 200−3200 cm^{-1} range. All solid samples were analyzed at both ambient temperature and low temperature ($T < T_g$), by placement on a surface filled with a NH_4Cl−ice water mixture. To confirm conversion below the T_g for the low-temperature reading and to ensure its state for the entirety of the acquisition period, the foam was fixed in a folded, constrained shape. Thermal equilibrium was ensured in all of the cases by maintaining the specimen under constant corresponding temperature for 5 min. Outputs are given relative to a 10 s integration time and 100% laser intensity. The band position and band intensity of the characteristic absorption peaks of the specimen were calculated by a Lorentzian curve-fitting procedure.[114] At least five positions on each sample were scanned at each temperature, with near-identical profiles. Attenuated total reflectance FTIR (ATR-FTIR) spectroscopy was carried out on a PerkinElmer Spectrum 100. Measurements were done over the 4000−650 cm^{-1} range, at a resolution of 4 cm^{-1}, with 20 scans per sample reading. Both TPU and SMPu solid samples were analyzed under ambient conditions. Results were ATR-corrected and baseline-subtracted using the onboard PerkinElmer Spectrum 100 software.

Chemical compositions of the final SMPu foam product were determined by liquid proton nuclear magnetic resonance (^{1}H NMR) spectroscopy. Samples were analyzed on a Jeol ECZ 500 MHz NMR spectrometer operating at 495.13 MHz equipped with a double-resonance 5 mm Royal probe at 298 K. A total of 16−128 free induction decays (FIDs) were collected into 16 K data points with a spectral width of 9615.38 Hz (16 ppm). A 2 s relaxation delay is used between pulses. Spectra

DOI: 10.1021/acsomega.9b01167
ACS Omega 2019, 4, 15348−15358

were analyzed in Delta (Jeol Ltd.). FIDs were zero-filled to 32 K, and an exponential line-broadening function of 0.2 Hz was applied to the FID prior to Fourier transformation. All of the sample spectra were phased and manually baseline-corrected, and spectra were referenced to trimethylsilane internal standard.

4.1.2. Shape Memory Property Testing. The fixity of the SMPu foam to different shapes and the shape recovery process were performed under both load-free and constrained (loaded) conditions. To fix a new shape, e.g., a shorter size, a cylindrical foam specimen was compressed at a "high" temperature ($T > T_g$; ~40 °C) to a corresponding strain (ε_u) on the Instron Compression tester. Then, the compressed foam was cooled down to well below the transition temperature ($T < T_g$; ~0 °C), and the foam was isothermally unloaded to zero stress level, to check the fixed strain level (ε_m). For the original shape recovery, the fixed foam was heated at high temperature ($T > T_g$), and both time and strain were recorded to examine the recovery process under a load-free state. This cycle of thermomechanical fixity and recovery was repeated five consecutive times to confirm repeatability. In addition to load-free shape recovery, constrained recovery testing was also conducted to obtain the amount of the recovery stress stored in the foam after fixity. The recovery stresses at different fixed strains (ε_m) were also measured. In addition to the use of Instron compression plates for deformation, other objects with spherical or sharp shapes were also used for memory testing to yield complex concavities of different shapes at selective foam sites.

4.1.3. Pressure (Re)Distribution Measurement. Two simple laboratory methods were employed for measurement of pressure distribution at the interfacial contact between the foam and the indenter. The first method used a spherical object indenting the foam under isothermal conditions (Figure 7), and the amount of contact area and the depth of penetration (from the top surface) marked between them were obtained.[37] Using the immersion data, the pressure was calculated from the ratio of the object mass and the interfacial area of contact. The SMPu foam can be easily programmed (fixed) to different shapes, as explained in Section 2.3; varying concavity levels were fixed on the foam surface, and the interfacial pressure with the spherical object was analyzed.

The second method of studying the interfacial contact includes an active measurement of the interfacial pressure distributions at different temperatures. The Tekscan *F*-scan foot pressure measurement system was used, consisting of several pressure points arranged on a flat film surface (Figure S1). First, the *F*-scan foot system was calibrated by an individual male volunteer after performing several initial trails under "walking calibration". After calibration, the SMPu foam was placed over the pressure sensor and the individual stood still and stationary on the foam surface. The pressure data were transmitted in real time to a computer via a WiFi channel. The pressure distributions on the foam surface heated to different temperatures were recorded. Due to limited foam size available for the experiment, only the area of the plantar fasciitis (i.e., underneath the heel) was used in the analysis.

■ ASSOCIATED CONTENT

Supporting Information

The Supporting Information is available free of charge on the ACS Publications website at DOI: 10.1021/acsomega.9b01167.

Mechanistic overview; ATR-FTIR spectra; variable-temperature Raman spectra; ^{1}H NMR spectra; DSC curves; XRD patterns; and TGA thermograms and data tables (PDF)

■ AUTHOR INFORMATION

Corresponding Author

*E-mail: nmnoor@polyu.edu.hk.

ORCID

Nuruzzaman Noor: 0000-0003-1897-1529

Ning Pan: 0000-0002-8772-2596

Notes

The authors declare no competing financial interest.

■ ACKNOWLEDGMENTS

The authors thank Dr. Patrick Pang, Lab Manager of the HK PolyU ITC Materials Processing Department, for his invaluable help and assistance with ATR-FTIR, Raman, DSC, TGA, and general lab processes, as well as acknowledge the support from the HK PolyU University Research Facility on Chemical and Environmental Analysis (URFCE). They thank Dr. Nurulamin Noor, NIHR Academic Clinical Fellow in Medicine at the Cambridge Immunology Network, University of Cambridge, and Dr. Ameersing Luximon of the Hong Kong Ergonomics Society, for invaluable discussions and comments. They acknowledge the financial support received from the Department of Science and Technology, India (#RP03454) and The Hong Kong Polytechnic University (1-ZVK4 and 1-ZVLR).

■ REFERENCES

(1) Lendlein, A.; Gould, O. E. C. Reprogrammable Recovery and Actuation Behaviour of Shape-Memory Polymers. *Nat. Rev. Mater.* **2019**, *4*, 116−133.

(2) Hager, M. D.; Bode, S.; Weber, C.; Schubert, U. S. Shape Memory Polymers: Past, Present and Future Developments. *Prog. Polym. Sci.* **2015**, *49*−*50*, 3−33.

(3) Sun, L.; Huang, W. M.; Ding, Z.; Zhao, Y.; Wang, C. C.; Purnawali, H.; Tang, C. Stimulus-Responsive Shape Memory Materials: A Review. *Mater. Des.* **2012**, *33*, 577−640.

(4) Hu, J.; Zhu, S.; Young, R. J.; Cai, Z.; Li, L.; Han, J.; Pan, N. Stress Memory Materials and Their Fundamental Platform. *J. Mater. Chem. A* **2017**, *5*, 503−511.

(5) Behl, M.; Razzaq, M. Y.; Lendlein, A. Multifunctional Shape-Memory Polymers. *Adv. Mater.* **2010**, *22*, 3388−3410.

(6) Behl, M.; Lendlein, A. Shape-Memory Polymers. *Mater. Today* **2007**, *10*, 20−28.

(7) Yao, Y.; Luo, Y.; Xu, Y.; Wang, B.; Li, J.; Deng, H.; Lu, H. Fabrication and Characterization of Auxetic Shape Memory Composite Foams. *Composites, Part B* **2018**, *152*, 1−7.

(8) Kim, H. M.; Huang, Z. M.; Kim, J. S.; Youn, J. R.; Song, Y. S. Fabrication and Analysis of Dual-Scaled Shape Memory Foam. *Eur. Polym. J.* **2018**, *106*, 188−195.

(9) Hasan, S. M.; Nash, L. D.; Maitland, D. J. Porous Shape Memory Polymers: Design & Applications. *J. Polym. Sci., Part B: Polym. Phys.* **2016**, *54*, 1300−1318.

(10) Leng, J.; Lan, X.; Liu, Y.; Du, S. Shape-Memory Polymers & Their Composites: Stimulus Methods & Applications. *Prog. Mater. Sci.* **2011**, *56*, 1077−1135.

(11) Yu, K.; Ge, Q.; Qi, H. J. Reduced Time as a Unified Parameter Determining Fixity and Free Recovery of Shape Memory Polymers. *Nat. Commun.* **2014**, *5*, No. 3066.

(12) Lendlein, A.; Kelch, S. Shape-Memory Polymers. *Angew. Chem., Int. Ed.* **2002**, *41*, 2034.

DOI: 10.1021/acsomega.9b01167
ACS Omega 2019, 4, 15348−15358

(13) Hardy, J. G.; Palma, M.; Wind, S. J.; Biggs, M. J. Responsive Biomaterials: Advances in Materials Based on Shape-Memory Polymers. *Adv. Mater.* **2016**, 5717−5724.
(14) Chan, B. Q. Y.; Low, Z. W. K.; Heng, S. J. W.; Chan, S. Y.; Owh, C.; Loh, X. J. Recent Advances in Shape Memory Soft Materials for Biomedical Applications. *ACS Appl. Mater. Interfaces* **2016**, *8*, 10070−10087.
(15) Sehmi, S. K.; Noimark, S.; Weiner, J.; Allan, E.; MacRobert, A. J.; Parkin, I. P. Potent Antibacterial Activity of Copper Embedded into Silicone & Polyurethane. *ACS Appl. Mater. Interfaces* **2015**, *7*, 22807−22813.
(16) Gong, T.; Zhao, K.; Liu, X.; Lu, L.; Liu, D.; Zhou, S. A Dynamically Tunable, Bioinspired Micropatterned Surface Regulates Vascular Endothelial and Smooth Muscle Cells Growth at Vascularization. *Small* **2016**, *12*, 5769−5778.
(17) Han, Y.; Hu, J.; Jiang, L. Collagen Skin, a Water-Sensitive Shape Memory Material. *J. Mater. Chem. B* **2018**, *6*, 5144−5152.
(18) Gök, M. O.; Bilir, M. Z.; Gürcüm, B. H. Shape-Memory Applications in Textile Design. *Procedia − Soc. Behav. Sci.* **2015**, *195*, 2160−2169.
(19) Lv, T.; Cheng, Z.; Zhang, E.; Kang, H.; Liu, Y.; Jiang, L. Self-Restoration of Superhydrophobicity on Shape Memory Polymer Arrays with Both Crushed Microstructure and Damaged Surface Chemistry. *Small* **2017**, *13*, No. 1503402.
(20) Venkatesan, H.; Hu, J.; Chen, J. Bioinspired Fabrication of Polyurethane/Regenerated Silk Fibroin Composite Fibres with Tubuliform Silk-Like Flat Stress−Strain Behaviour. *Polymers* **2018**, *10*, No. 333.
(21) Liu, Y.; Du, H.; Liu, L.; Leng, J. Shape Memory Polymers and Their Composites in Aerospace Applications: A Review. *Smart Mater. Struct.* **2014**, *23*, No. 023001.
(22) Zarek, M.; Layani, M.; Cooperstein, I.; Sachyani, E.; Cohn, D.; Magdassi, S. 3D Printing of Shape Memory Polymers for Flexible Electronic Devices. *Adv. Mater.* **2016**, *28*, 4449−4454.
(23) Lendlein, A. Biodegradable, Elastic Shape-Memory Polymers for Potential Biomedical Applications. *Science* **2002**, *296*, 1673−1676.
(24) Wache, H. M.; Tartakowska, D. J.; Hentrich, A.; Wagner, M. H. Development of a Polymer Stent with Shape Memory Effect as a Drug Delivery System. *J. Mater. Sci.: Mater. Med.* **2003**, *14*, 109−112.
(25) Singhal, P.; Small, W.; Cosgriff-Hernandez, E.; Maitland, D. J.; Wilson, T. S. Low Density Biodegradable Shape Memory Polyurethane Foams for Embolic Biomedical Applications. *Acta Biomater.* **2014**, *10*, 67−76.
(26) Serrano, M. C.; Carbajal, L.; Ameer, G. A. Novel Biodegradable Shape-Memory Elastomers with Drug-Releasing Capabilities. *Adv. Mater.* **2011**, *23*, 2211−2215.
(27) Ng, S.-W.; Noor, N.; Zheng, Z. Graphene-Based Two-Dimensional Janus Materials. *NPG Asia Mater.* **2018**, *10*, 217−237.
(28) Neuss, S.; Blomenkamp, I.; Stainforth, R.; Boltersdorf, D.; Jansen, M.; Butz, N.; Perez-Bouza, A.; Knüchel, R. The Use of a Shape-Memory Poly(E{lunate}-Caprolactone)Dimethacrylate Network as a Tissue Engineering Scaffold. *Biomaterials* **2009**, *30*, 1697−1705.
(29) Wu, X.; Mahalingam, S.; VanOosten, S. K.; Wisdom, C.; Tamerler, C.; Edirisinghe, M. New Generation of Tunable Bioactive Shape Memory Mats Integrated with Genetically Engineered Proteins. *Macromol. Biosci.* **2017**, *17*, No. 1600270.
(30) Kumar, B.; Hu, J.; Pan, N. Smart Medical Stocking Using Memory Polymer for Chronic Venous Disorders. *Biomaterials* **2016**, *75*, 174−181.
(31) Narayana, H.; Hu, J.; Kumar, B.; Shang, S.; Han, J.; Liu, P.; Lin, T.; Ji, F.; Zhu, Y. Stress-Memory Polymeric Filaments for Advanced Compression Therapy. *J. Mater. Chem. B* **2017**, *5*, 1905−1916.
(32) Kumar, B.; Pan, N.; Hu, J. L. Shape Memory Compression System for Management of Chronic Venous Disorders. *Smart Text. Appl.* **2016**, 145−159.
(33) Hu, J.; Kumar, B.; Narayana, H. Stress Memory Polymers. *J. Polym. Sci., Part B: Polym. Phys.* **2015**, *53*, 893−898.
(34) Edsberg, L. E.; Black, J. M.; Goldberg, M.; McNichol, L.; Moore, L.; Sieggreen, M. Revised National Pressure Ulcer Advisory Panel Pressure Injury Staging System: Revised Pressure Injury Staging System. *J Wound Ostomy Cont. Nurs.* **2016**, *43*, 585−597.
(35) Chou, R.; Dana, T.; Bougatsos, C.; Blazina, I.; Starmer, A. J.; Reitel, K.; Buckley, D. I. Pressure Ulcer Risk Assessment & Prevention: A Systematic Comparative Effectiveness Review. *Ann. Intern. Med.* **2013**, *159*, 28−38.
(36) Ahmad, M.; Luo, J.; Miraftab, M. Feasibility Study of Polyurethane Shape-Memory Polymer Actuators for Pressure Bandage Application. *Sci. Technol. Adv. Mater.* **2012**, *13*, No. 015006.
(37) Bader, D. Laboratory Measurement of the Interface Pressures Applied by Active Therapy Support Surfaces: A Consensus Document. *J. Tissue Viability* **2010**, *19*, 2−6.
(38) Tobushi, H.; Okumura, K.; Endo, M.; Hayashi, S. Thermomechanical Properties of Polyurethane-Shape Memory Polymer Foam. *J. Intell. Mater. Syst. Struct.* **2001**, *12*, 283−287.
(39) Tobushi, H.; Shimada, D.; Hayashi, S.; Endo, M. Shape Fixity and Shape Recovery of Polyurethane Shape-Memory Polymer Foams. *Proc. Inst. Mech. Eng., Part L* **2003**, *217*, 135−143.
(40) Santo, L. Shape Memory Polymer Foams. *Prog. Aerosp. Sci.* **2016**, *81*, 60−65.
(41) Kang, S. M.; Lee, S. J.; Kim, B. K. Shape Memory Polyurethane Foams. *Express Polym. Lett.* **2012**, *6*, 63−69.
(42) Jiang, L.; Hu, H. Finite Element Modeling of Multilayer Orthogonal Auxetic Composites under Low-Velocity Impact. *Materials* **2017**, *10*, No. 908.
(43) Li, G. *Self-Healing Composites: Shape Memory Polymer-Based Structures*; John Wiley & Sons, 2014.
(44) Ahmed, M. F.; Li, Y.; Yao, Z.; Cao, K.; Zeng, C. TPU/PLA Blend Foams: Enhanced Foamability, Structural Stability, and Implications for Shape Memory Foams. *J. Appl. Polym. Sci.* **2019**, *136*, No. 47416.
(45) Menon, A. V.; Madras, G.; Bose, S. Shape Memory Polyurethane Nanocomposites with Porous Architectures for Enhanced Microwave Shielding. *Chem. Eng. J.* **2018**, *352*, 590−600.
(46) Weems, A. C.; Li, W.; Maitland, D. J.; Calle, L. M. Polyurethane Microparticles for Stimuli Response and Reduced Oxidative Degradation in Highly Porous Shape Memory Polymers. *ACS Appl. Mater. Interfaces* **2018**, *10*, 32998−33009.
(47) Zhang, Y.; Li, Y.; Liu, W. Dipole-Dipole & h-Bonding Interactions Significantly Enhance the Multifaceted Mechanical Properties of Thermoresponsive Shape Memory Hydrogels. *Adv. Funct. Mater.* **2015**, *25*, 471−480.
(48) Pei, Z.; Yang, Y.; Chen, Q.; Wei, Y.; Ji, Y. Regional Shape Control of Strategically Assembled Multishape Memory Vitrimers. *Adv. Mater.* **2016**, *28*, 156−160.
(49) Guo, M.; Pitet, L. M.; Wyss, H. M.; Vos, M.; Dankers, P. Y. W. W.; Meijer, E. W. Tough Stimuli-Responsive Supramolecular Hydrogels with Hydrogen-Bonding Network Junctions. *J. Am. Chem. Soc.* **2014**, *136*, 6969−6977.
(50) Fang, C.; Leng, J.; Sun, H.; Gu, J. A Multi-Branch Thermoviscoelastic Model Based on Fractional Derivatives for Free Recovery Behaviors of Shape Memory Polymers. *Mech. Mater.* **2018**, *120*, 34−42.
(51) Mak, A. F. T.; Zhang, M.; Tam, E. W. C. Biomechanics of Pressure Ulcer in Body Tissues Interacting with External Forces during Locomotion. *Annu. Rev. Biomed. Eng.* **2010**, *12*, 29−53.
(52) Amano, Y.; Hidema, R.; Gong, J.; Furukawa, H. Creation of Shape-Memory Gels with Inter-Crosslinking Network Structure. *Chem. Lett.* **2012**, *41*, 1029−1031.
(53) Miaudet, P.; Derre, A.; Maugey, M.; Zakri, C.; Piccione, P. M.; Inoubli, R.; Poulin, P. Shape and Temperature Memory of Nanocomposites with Broadened Glass Transition. *Science* **2007**, *318*, 1294−1296.
(54) Meng, Y.; Jiang, J.; Anthamatten, M. Body Temperature Triggered Shape-Memory Polymers with High Elastic Energy Storage Capacity. *J. Polym. Sci., Part B: Polym. Phys.* **2016**, *54*, 1397−1404.

DOI: 10.1021/acsomega.9b01167
ACS Omega 2019, 4, 15348−15358

(55) Duscher, D.; Neofytou, E.; Wong, V. W.; Maan, Z. N.; Rennert, R. C.; Inayathullah, M.; Januszyk, M.; Rodrigues, M.; Malkovskiy, A. V.; Whitmore, A. J.; Walmsley, G. G.; Galvez, M. G.; Whittam, A. J.; Brownlee, M.; Rajadas, J.; Gurtner, G. C. Transdermal Deferoxamine Prevents Pressure-Induced Diabetic Ulcers. *Proc. Natl. Acad. Sci. U.S.A.* **2015**, *112*, 94−99.
(56) Amin, N.; Doupis, J. Diabetic Foot Disease: From the Evaluation of the "Foot at Risk" to the Novel Diabetic Ulcer Treatment Modalities. *World J. Diabetes* **2016**, *7*, 153.
(57) Urbancic-Rovan, V. Causes of Diabetic Foot Lesions. *Lancet* **2005**, *366*, 1675−1676.
(58) World Health Organization. *Global Report on Diabetes*; WHO, 2016; Vol. *978*.
(59) Hall, M.; Shurr, D. G.; Zimmerman, M. B.; Saltzman, C. L. Plantar Foot Surface Temperatures with Use of Insoles. *Iowa Orthop. J.* **2004**, *24*, 72−75.
(60) Andrieux, S.; Quell, A.; Stubenrauch, C.; Drenckhan, W. Liquid Foam Templating − A Route to Tailor-Made Polymer Foams. *Adv. Colloid Interface Sci.* **2018**, *256*, 276−290.
(61) Barmouz, M.; Behravesh, A. H. The Role of Foaming Process on Shape Memory Behavior of Polylactic Acid-Thermoplastic Polyurethane-Nano Cellulose Bio-Nanocomposites. *J. Mech. Behav. Biomed. Mater.* **2019**, *91*, 266−277.
(62) Floros, M.; Hojabri, L.; Abraham, E.; Jose, J.; Thomas, S.; Pothan, L.; Leao, A. L.; Narine, S. Enhancement of Thermal Stability, Strength and Extensibility of Lipid-Based Polyurethanes with Cellulose-Based Nanofibers. *Polym. Degrad. Stab.* **2012**, *97*, 1970−1978.
(63) Zhu, Y.; Hu, J.; Luo, H.; Young, R. J.; Deng, L.; Zhang, S.; Fan, Y.; Ye, G. Rapidly Switchable Water-Sensitive Shape-Memory Cellulose/Elastomer Nano-Composites. *Soft Matter* **2012**, *8*, 2509.
(64) Braun, B.; Dorgan, J. R.; Dec, S. F. Infrared Spectroscopic Determination of Lactide Concentration in Polylactide: An Improved Methodology. *Macromolecules* **2006**, *39*, 9302−9310.
(65) Liu, X.; Wang, T.; Li, J.; Cheng, J.; Zhang, J. Synthesis and Properties of Segmented Polyurethanes with Hydroquinone Ether Derivatives as Chain Extender. *J. Polym. Res.* **2015**, *22*, No. 149.
(66) Leitsch, E. K.; Beniah, G.; Liu, K.; Lan, T.; Heath, W. H.; Scheidt, K. A.; Torkelson, J. M. Nonisocyanate Thermoplastic Polyhydroxyurethane Elastomers via Cyclic Carbonate Aminolysis: Critical Role of Hydroxyl Groups in Controlling Nanophase Separation. *ACS Macro Lett.* **2016**, *5*, 424−429.
(67) Parnell, S.; Min, K.; Cakmak, M. Kinetic Studies of Polyurethane Polymerization with Raman Spectroscopy. *Polymer* **2003**, *44*, 5137−5144.
(68) Aust, J. F.; Higgins, M. K.; Groner, P.; Morgan, S. L.; Myrick, M. L. Fourier Transform Raman Spectroscopic Studies of a Polyimide Curing Reaction. *Anal. Chim. Acta* **1994**, *293*, 119−128.
(69) Cregut, M.; Bedas, M.; Assaf, A.; Durand-Thouand, M. J.; Thouand, G. Applying Raman Spectroscopy to the Assessment of the Biodegradation of Industrial Polyurethanes Wastes. *Environ. Sci. Pollut. Res.* **2014**, *21*, 9538−9544.
(70) Janik, H.; Pałys, B.; Petrovic, Z. S. Multiphase-Separated Polyurethanes Studied by Micro-Raman Spectroscopy. *Macromol. Rapid Commun.* **2003**, *24*, 265−268.
(71) Teo, L.-S.; Chen, C.-Y.; Kuo, J.-F. Fourier Transform Infrared Spectroscopy Study on Effects of Temperature on Hydrogen Bonding in Amine-Containing Polyurethanes & Poly(Urethane−urea)S. *Macromolecules* **1997**, *30*, 1793−1799.
(72) Pegoraro, M.; Galbiati, A.; Ricca, G. 1H Nuclear Magnetic Resonance Study of Polyurethane Prepolymers from Toluene Diisocyanate and Polypropylene Glycol. *J. Appl. Polym. Sci.* **2003**, *87*, 347−357.
(73) Brame, E. G.; Ferguson, R. C.; Thomas, G. J. Identification of Polyurethanes by High Resolution Nuclear Magnetic Resonance Spectrometry. *Anal. Chem.* **1967**, *39*, 517−521.
(74) Van Heumen, J. D.; Stevens, J. R. The Role of Lithium Salts in the Conductivity & Phase Morphology of a Thermoplastic Polyurethane. *Macromolecules* **1995**, *28*, 4268−4277.
(75) Datta, J.; Kasprzyk, P. Thermoplastic Polyurethanes Derived from Petrochemical or Renewable Resources: A Comprehensive Review. *Polym. Eng. Sci.* **2018**, *58*, E14−E35.
(76) Menard, K. P.; Menard, N. R. Dynamic Mechanical Analysis in the Analysis of Polymers and Rubbers. *Encyclopedia of Polymer Science and Technology*; John Wiley & Sons, Inc.: Hoboken, NJ, 2015; pp 1−33.
(77) Foreman, J.; Sauerbrunn, S. R.; Marcozzi, C. L. *Exploring the Sensitivity of Thermal Analysis Techniques to the Glass Transition Document Reference: TA082*; TA Instruments, Inc., 2006.
(78) Xu, Y.; Petrovic, Z.; Das, S.; Wilkes, G. L. Morphology and Properties of Thermoplastic Polyurethanes with Dangling Chains in Ricinoleate-Based Soft Segments. *Polymer* **2008**, *49*, 4248−4258.
(79) Liu, J.-C.; Martin, D. J.; Moon, R. J.; Youngblood, J. P. Enhanced Thermal Stability of Biomedical Thermoplastic Polyurethane with the Addition of Cellulose Nanocrystals. *J. Appl. Polym. Sci.* **2015**, *132*, No. 41970.
(80) Van Ekeren, P. J.; Carton, E. P. Polyurethanes for Potential Use in Transparent Armour Investigated Using DSC and DMA. *J. Therm. Anal. Calorim.* **2011**, *105*, 591−598.
(81) Chen, S.; Hu, J.; Liu, Y.; Liem, H.; Zhu, Y.; Meng, Q. Effect of Molecular Weight on Shape Memory Behavior in Polyurethane Films. *Polym. Int.* **2007**, *56*, 1128−1134.
(82) Li, S.; Zhao, J.; Zhang, Z.; Zhang, J.; Yang, W. Aliphatic Thermoplastic Polyurethane-Ureas and Polyureas Synthesized through a Non-Isocyanate Route. *RSC Adv.* **2015**, *5*, 6843−6852.
(83) Anandhan, S.; Lee, H. S. Influence of Organically Modified Clay Mineral on Domain Structure and Properties of Segmented Thermoplastic Polyurethane Elastomer. *J. Elastomers Plast.* **2014**, *46*, 217−232.
(84) Memarian, F.; Fereidoon, A.; Ghorbanzadeh Ahangari, M. The Shape Memory, & the Mechanical and Thermal Properties of TPU/ABS/CNT: A Ternary Polymer Composite. *RSC Adv.* **2016**, *6*, No. 101038.
(85) Bera, M.; Maji, P. K. Effect of Structural Disparity of Graphene-Based Materials on Thermo-Mechanical and Surface Properties of Thermoplastic Polyurethane Nanocomposites. *Polymer* **2017**, *119*, 118−133.
(86) Wang, J.; Yuan, B.; Mu, X.; Wang, W.; Hu, W.; Hu, Y. Novel Incorporation of Mesoporous $NiCo_2O_4$ into Thermoplastic Polyurethane for Enhancing Its Fire Safety. *RSC Adv.* **2016**, *6*, 109620−109632.
(87) Hou, Y.; Duan, L.; Gui, Z.; Hu, Y. An Infiltration Method to Synthesize Thermoplastic Polyurethane Composites Based on Size-Controlled Graphene Foams. *Composites, Part A* **2017**, *97*, 67−75.
(88) Polat, Y.; Pampal, E. S.; Stojanovska, E.; Simsek, R.; Hassanin, A.; Kilic, A.; Demir, A.; Yilmaz, S. Solution Blowing of Thermoplastic Polyurethane Nanofibers: A Facile Method to Produce Flexible Porous Materials. *J. Appl. Polym. Sci.* **2016**, *133*, No. 43025.
(89) Gundogdu, N. A. S.; Akgul, Y.; Kilic, A. Optimization of Centrifugally Spun Thermoplastic Polyurethane Nanofibers for Air Filtration Applications. *Aerosol Sci. Technol.* **2018**, *52*, 515−523.
(90) Vitkauskien, I.; Makuška, R.; Stirna, U.; Cabulis, U. Thermal Properties of Polyurethane-Polyisocyanurate Foams Based on Poly-(Ethylene Terephthalate) Waste. *Mater. Sci.* **2011**, *17*, 249−253.
(91) Lai, S.-M.; Wang, C.-K.; Shen, H.-F. Properties & Preparation of Thermoplastic Polyurethane/Silica Hybrid Using Sol-Gel Process. *J. Appl. Polym. Sci.* **2005**, *97*, 1316−1325.
(92) Ahmad, Z.; Ansell, M.; Smedley, D.; Tahir, P. M. Creep Behavior of Epoxy-Based Adhesive Reinforced with Nanoparticles for Bonded-In Timber Connection. *J. Mater. Civ. Eng.* **2012**, *24*, 825−831.
(93) Dutta, J.; Naskar, K. Investigation of Morphology, Mechanical, Dynamic Mechanical and Thermal Behaviour of Blends Based on Ethylene Vinyl Acetate (EVA) and Thermoplastic Polyurethane (TPU). *RSC Adv.* **2014**, *4*, 60831−60841.
(94) Mi, H.-Y.; Salick, M. R.; Jing, X.; Jacques, B. R.; Crone, W. C.; Peng, X.-F.; Turng, L.-S. Characterization of Thermoplastic Polyurethane/Polylactic Acid (TPU/PLA) Tissue Engineering Scaffolds

DOI: 10.1021/acsomega.9b01167
ACS Omega 2019, 4, 15348−15358

Fabricated by Microcellular Injection Molding. *Mater. Sci. Eng., C* **2013**, *33*, 4767−4776.
(95) Behera, P. K.; Usha, K. M.; Guchhait, P. K.; Jehnichen, D.; Das, A.; Voit, B.; Singha, N. K. A Novel Ionomeric Polyurethane Elastomer Based on Ionic Liquid as Crosslinker. *RSC Adv.* **2016**, *6*, 99404−99413.
(96) Saber-Sheikh, K.; Clarke, R. L.; Braden, M. Viscoelastic Properties of Some Soft Lining Materials. I-Effect of Temperature. *Biomaterials* **1999**, *20*, 817−822.
(97) Singhal, P.; Rodriguez, J. N.; Small, W.; Eagleston, S.; Van de Water, J.; Maitland, D. J.; Wilson, T. S. Ultra Low Density and Highly Crosslinked Biocompatible Shape Memory Polyurethane Foams. *J. Polym. Sci., Part B: Polym. Phys.* **2012**, *50*, 724−737.
(98) Patton, S.; Chen, C.; Hu, J.; Grazulis, L.; Schrand, A.; Roy, A. Characterization of Thermoplastic Polyurethane (TPU) and Ag-Carbon Black TPU Nanocomposite for Potential Application in Additive Manufacturing. *Polymers* **2017**, *9*, No. 6.
(99) Kanyanta, V.; Ivankovic, A. Mechanical Characterisation of Polyurethane Elastomer for Biomedical Applications. *J. Mech. Behav. Biomed. Mater.* **2010**, *3*, 51−62.
(100) Qu, X. Impacts of Different Types of Insoles on Postural Stability in Older Adults. *Appl. Ergon.* **2015**, *46*, 38−43.
(101) Scarfato, P.; Di Maio, L.; Incarnato, L. Structure and Physical-Mechanical Properties Related to Comfort of Flexible Polyurethane Foams for Mattress & Effects of Artificial Weathering. *Composites, Part B* **2017**, *109*, 45−52.
(102) Obi, B. E. In *Polymeric Foams Structure−Property−Performance: A Design Guide*; Obi, B. E., Ed.; William Andrew, 2017.
(103) Zheng, N.; Fang, Z.; Zou, W.; Zhao, Q.; Xie, T. Inside Cover: Thermoset Shape-Memory Polyurethane with Intrinsic Plasticity Enabled by Transcarbamoylation (Angew. Chem. Int. Ed. 38/2016). *Angew. Chem., Int. Ed.* **2016**, *55*, 11304.
(104) Brodsky, J. W.; Kourosh, S.; Stills, M.; Mooney, V. Objective Evaluation of Insert Material for Diabetic and Athletic Footwear. *Foot Ankle* **1988**, *9*, 111−116.
(105) Mittal, V.; Kim, J.-K.; Pal, K. *Recent Advances in Elastomeric Nanocomposites*; Springer, 2011.
(106) Liu, C.; Zong, R.; Chen, H.; Wang, J.; Wu, C. Comparative Study of Toxicity for Thermoplastic Polyurethane and Its Flame-Retardant Composites. *J. Thermoplast. Compos. Mater.* **2019**, 1393−1407.
(107) Liu, X.; Hao, J.; Gaan, S. Recent Studies on the Decomposition and Strategies of Smoke and Toxicity Suppression for Polyurethane Based Materials. *RSC Adv.* **2016**, *6*, 74742−74756.
(108) McKenna, S. T.; Hull, T. R. The Fire Toxicity of Polyurethane Foams. *Fire Sci. Rev.* **2016**, *5*, No. 3.
(109) Wise, D. L., Trantolo, D. J., Altobelli, D. E., Yaszemski, M. J., Gresser, J. D., Eds. *Human Biomaterials Applications*, 2nd ed.; Humana Press, 2013.
(110) Gogoi, S.; Barua, S.; Karak, N. Cross-Linking Kinetics of Hyperbranched Epoxy Cured Hyperbranched Polyurethane and Optimization of Reaction Conversion by Central Composite Design. *Chem. Eng. Sci.* **2015**, *127*, 230−238.
(111) Chattopadhyay, D. K.; Sreedhar, B.; Raju, K. V. S. N. Effect of Chain Extender on Phase Mixing and Coating Properties of Polyurethane Ureas. *Ind. Eng. Chem. Res.* **2005**, *44*, 1772−1779.
(112) Delpech, M. C.; Coutinho, F. M. B. Waterborne Anionic Polyurethanes and Poly(Urethane-Urea)s: Influence of the Chain Extender on Mechanical and Adhesive Properties. *Polym. Test.* **2000**, *19*, 939−952.
(113) Choi, J.; Moon, D. S.; Jang, J. U.; Yin, W. B.; Lee, B.; Lee, K. J. Synthesis of Highly Functionalized Thermoplastic Polyurethanes and Their Potential Applications. *Polymer* **2017**, *116*, 287−294.
(114) Wojdyr, M. Fityk: A General-Purpose Peak Fitting Program. *J. Appl. Crystallogr.* **2010**, *43*, 1126−1128.

DOI: 10.1021/acsomega.9b01167
ACS Omega 2019, 4, 15348−15358